CHALMERS
UNIVERSITY OF TECHNOLOGY

Measuring and modeling material properties during high loading rates

Material characterization of A36 steel under high loading rates using the Split Hopkinson Pressure Bar and numerical modeling

Master's thesis in Applied Mechanics

FRIDA KROHN

Department of Industrial and Materials Science

CHALMERS UNIVERSITY OF TECHNOLOGY
Gothenburg, Sweden 2025
www.chalmers.se

Master's thesis 2025

Measuring and modeling material properties during high loading rates

Material characterization of A36 steel under high loading rates using the Split Hopkinson Pressure Bar and numerical modeling

FRIDA KROHN

CHALMERS
UNIVERSITY OF TECHNOLOGY

Department of Industrial and Materials Science
Division of Material & Computational Mechanics
Chalmers University of Technology
Gothenburg, Sweden 2025

Measuring and modeling material properties during high loading rates
Material characterization of A36 steel under high loading rates using the Split Hopkinson Pressure Bar and numerical modeling
FRIDA KROHN

© FRIDA KROHN, 2025.

Supervisor: Gengsheng Wang, FOI
Examiner: Magnus Ekh, Department of Industrial and Materials Science

Master's Thesis 2025
Department of Industrial and Materials Science
Division of Material & Computational Mechanics
Chalmers University of Technology
SE-412 96 Gothenburg
Telephone +46 31 772 1000

Typeset in LaTeX
Printed by Chalmers Reproservice
Gothenburg, Sweden 2025

Measuring and modeling material properties during high loading rates
Material characterization of A36 steel under high loading rates using the Split Hopkinson Pressure Bar and numerical modeling
FRIDA KROHN
Department of Industrial and Materials Science
Chalmers University of Technology

Abstract

This thesis aims to evaluate a method for analyzing the high strain rate behavior of A36 steel by combining experimental testing and numerical modeling. Experiments consisting of uniaxial compressive tests and Split Hopkinson Pressure bar tests were performed to cover low and high strain rates. The method's ability to use low strain rate data to predict high strain rate behavior using the Johnson-Cook material model was evaluated. Numerical modeling and parameter optimization were performed in LS-DYNA and LS-OPT, respectively. The results showed reasonable agreement between the experiments and simulations for hydraulic compressive and Split Hopkinson Pressure Bar tests. Consistently, an explicit strain rate dependency is present throughout the tests, but fluctuations in the Split Hopkinson Pressure Bar data complicated the data analysis. The method has strengths and limitations. While the Johnson-Cook material model effectively models A36 steel at high strain rates, additional refinements in the numerical model and parameter optimization process are needed to obtain a reliable set of parameter values. Improving the reliability of the strain gauge data and introducing striker velocity measurements could elevate future method development. In this thesis, the method chosen to evaluate steel's high strain rate behavior provides a foundation for further work. Refinements in experimental setup and numerical modeling are necessary to improve the reliability of the results before they can be applied effectively in future studies.

Keywords: Split Hopkinson Pressure Bar, SHPB, A36, Johnson-Cook

Sammanfattning

Detta examensarbete syftar till att utvärdera en metod för att analysera beteendet vid höga belastningshastigheter hos A36-stål genom en kombination av experimentella tester och numerisk modellering. Experimentella tester i form av enaxiella tryckprov och Split Hopkinson Pressure Bar-tester genomfördes för att täcka både låga och höga deformationshastigheter. Metodens förmåga att använda data från låga deformationshastigheter för att förutsäga beteendet vid höga deformationshastigheter utvärderades med hjälp av materialmodellen Johnson-Cook. Numerisk modellering och parameteroptimering utfördes i LS-DYNA respektive LS-OPT. Resultaten visade en rimlig överensstämmelse mellan experiment och simuleringar för både hydrauliska tryckprov och Split Hopkinson Pressure Bar tester. Ett enhetligt och tydligt deformationshastighetsberoende kunde observeras, men svängningar i mätdatan från Split Hopkinson Pressure Bar-testerna försvårade analysen. Metoden har både styrkor och svagheter. Johnson-Cooks materialmodell modellerade effektivt beteendet hos A36-stål vid höga deformationshastigheter, men ytterligare förbättringar i den numeriska modellen och parameteroptimeringsprocessen krävs för att erhålla en tillförlitlig parameteruppsättning. För att förbättra metoden bör tillförlitligheten vid datainsamling med trådtöjningsgivarna förbättras samt hastighetsmätningar för strikern införas. Metoden som använts i detta examensarbete för att utvärdera ståls beteende vid höga belastningshastigheter kan används som grund för framtida arbete. Förbättringar i den experimentella uppställningen och den numeriska modelleringen är nödvändiga för att öka reultatens tillförlitlighet innan de efektivt kan tillämpas i framtida studier.

Acknowledgements

I would like to thank my supervisor Gengsheng Wang for the support during this project as well as the other people at FOI for their guidance, especially Mattias Unosson, Richard Malm and Håkan Hansson. I would also like to thank my examiner Magnus Ekh for his encouragement. Lastly I would like to thank my friends at Chalmers for making my time as a student memorable.

Frida Krohn, Stockholm, 2025

Contents

1
Introduction

Understanding how metals respond to dynamic loading is crucial in engineering applications, as it directly affects the performance and safety of components and structures, especially under high loading rates. Various experimental methods are commonly used to assess the behavior of materials subjected to high strain rates, one of which is the Split Hopkinson Pressure Bar (SHPB). This thesis investigates a method of analyzing the dynamic behavior of A36 steel [1]. This chapter describes the background and development of the Split Hopkinson pressure bar and describes the aim and objective of this thesis, which will provide the basis for the experimental and numerical work later presented.

1.1 Material testing and the history of the Split Hopkinson Pressure Bar

There are many handbooks listing material properties. These properties are usually obtained from quasi-static testing under standardized conditions. A regular compression test can provide reliable values for the material's yield point and ultimate strength [2]. While useful, these quasi-static properties offer little assurance of a product's performance in the real world, where it might experience being dropped on the ground or submitted to explosive blast. What both of these scenarios have in common is a load varying over time, leading to another aspect of material testing, how a material behaves under dynamic loading.

Using regular hydraulic-driven material testing techniques, problems arise quite quickly when increasing the velocity of the applied load, since there is a loss of accuracy and difficulties in keeping the circumstances controlled [2]. In a perspective of strain rate, a 5 mm long specimen being subjected to a displacement load of 1 m/s equals a strain rate of 200 1/s, while 10 m/s results in a strain rate of 2000 1/s, whereas the strain rate of the quasi-static material properties earlier mentioned is about 10^{-3} 1/s or lower. To be able to test materials at higher loading rates, with strain rates of about a few thousand per second, other approaches, like the SHPB, are needed to maintain control of the applied load while still collecting necessary data in a reliable way.

The challenges of high strain rate testing were historically approached by Hopkinson and Kolsky among several others. Their work led to the development of testing methods with the ability to examine material behaviors at high loading rates.

Hopkinson published a method for measuring stress pulses in metal bars in 1914, which led to the creation of a device now referred to as the Hopkinson pressure bar. His method was modified by Landon and Quinney in 1923 and further developed by Davies in 1948 [3]. In 1949, Kolsky published the article titled '*An Investigation of the Mechanical Properties of Materials at Very High Rates of Loading*', which has since then been widely cited. In the article's introduction, Kolsky refers back to earlier work where it was determined that the mechanical behavior of materials is dependent on the loading rate. These experiments were performed on plastics, rubber, copper, and lead. At very high rates of loading, two problems tend to arise. The first issue is handling the stress and strain components that do not act in the direction of loading. The second issue is the inertia effects in the setup, with one consequence being that it is almost impossible to separate the inertia effects from the studied material properties. Another consequence is that the stress along the specimen's length will be non-uniform due to its inertia [4]. Using the work of his fellow scientists, Kolsky developed the method used in his article by combining two Hopkinson bars with a thin specimen sandwiched between them, creating the setup now known as a Kolsky bar or more commonly referred to as the *Split* Hopkinson pressure bar. Using this method, inertia effects could be accounted for, and the thin specimen minimized the transverse stress and strain components. Therefore it is a useful method for material characterization. Even though extensive testing standards exist, there is still room for improvement regarding interpreting data and choosing a suitable material model for the application. One method of doing so will be explored in this thesis through a combination of experimental testing and numerical modeling.

1.2 Aim and objectives

This thesis aims to assess how hydraulic compression tests and Split Hopkinson Pressure Bar (SHPB) tests, together with the Johnson-Cook material model, contribute to accurately modeling the high strain rate behaviour of A36 steel.

In this thesis, both SHPB and regular hydraulic compression tests at different strain rates are performed. The accuracy of the Johnson-Cook material model will be evaluated by its ability to predict the steel's behavior in the range from quasi-static to dynamic strain rates. Numerical FEM models will be developed, and a model for parameter optimization will be used to derive suitable values for the material parameters in the Johnson-Cook material model. These models will be used to evaluate the ability to predict high strain rate behavior using low strain rate data.

1.3 Limitations

This study has several limitations, and these need to be acknowledged. These limitations include the experimental setup, material model and approach to numerical modelling.

The experimental section of this study has a few different limiting factors. The testing will be limited to A36 steel which is well studied and provides a good basis for comparison of the results, but limits the generalizability of the method. The specimens available have the same size, so the geometric effects will be accounted for using available theories. This study primarily relies on strain gauge data to evaluate the SHPB results since they have high sensitivity, accuracy, and the extracted data is straight forward to process. The strain gauges can however be sensitive to external noise and the rapid changes occurring at high loading rates may affect the accuracy of the measurements.

In this thesis, the numerical modeling is limited to examining one material model, the Johnson-Cook model, which may not be able to capture the material behaviors observed during testing. While using a well known and regularly used material model provides more data for comparison and evaluation, this also narrows the scope of the thesis.

These limitations will affect and influence the way the results are interpreted as well as help identify areas for improvement.

2
Behavior of metals

Metals can deform both elastically and plastically, depending on the applied stresses and loading conditions. It is common for a metal to transition between these two types of deformation during different stages of loading. Some metals may even harden during loading, and thereby increasing its strength. In this chapter, several phenomena that occur during compressive testing are presented.

2.1 Quasi-static conditions

Performing measurements on a system when it is in, or close to, equilibrium the quasi-static behavior is observed, this is achieved when the load is applied at a very slow rate. For a process to be considered quasi-static, it has to be sufficiently slow for the behavior of the material to appear close to as if it is under static conditions, meaning there is a low acceleration so the inertia is negligible.

The quasi-static state is different from the static state because of dynamic effects acting on the system, but these effects are generally so small that they can be neglected. For metals, testing is considered quasi-static for strain rates up to $\dot{\epsilon} = 2.5 \cdot 10^{-3}$ 1/s according to AMTS standards, which provides conditions for standardized material testing [5]. Quasi-static testing is fundamental for understanding material behavior as it serves as a reference for understanding changes occurring when dynamic effects are introduced.

2.2 Plasticity phenomena

Plastic deformation in metals is influenced by several phenomena: hardening, strain rate sensitivity, and yield drop are some of them. Each of these will influence the material's response during plastic loading.

Hardening

Hardening of metals occurs due to plastic deformation. When the material hardens, the ultimate strength increases. Plastic deformation occurs when the applied stress is sufficient to break the inter-atomic bonds, thus rearranging the atoms in the material. Before the rearrangement, the metal atoms have a mostly regular positioning. After the deformation, where there are dislocations, they develop a resistance to

further dislocations to form and propagate, making it harder to further deform the material.

Strain rate sensitivity

Strain rate sensitivity refers to a material's changed behavior for loadings with different strain rates. For lower strain rates, near the quasi-static region, the strain rate sensitivities are caused by the inertness of the developing dislocations, which can be related to a material relaxation time. Going into the dynamic region the same phenomenon becomes even more prominent. In the dynamic region, other strain rate effects also start to appear due to changes in the plastic flow close to areas of concentrated stress or variety in the material's microstructure, which is highly apparent in steels [6]. These effects influence the material strength, and they become more prominent as the strain rate increases.

Yield drop and Lüder bands

The transition between the elastic and plastic behavior of many metals shows a yield drop in the stress-strain curve. This phenomenon is not necessarily the material's actual behavior and occurs because of local deformations in the specimen [7]. These deformations are often called Lüder bands, and their shape varies with specimen geometry. The Lüder bands do not contribute to strain hardening before the whole specimen has plastically deformed since the bands develop at an almost constant level of stress [8].The bands show their presence in the stress-strain curve as a fluctuating region of almost constant average stress right after the higher yield point [7]. Both the yield drop and constant stress area are circled in the sketched stress-strain curve in Figure 2.1

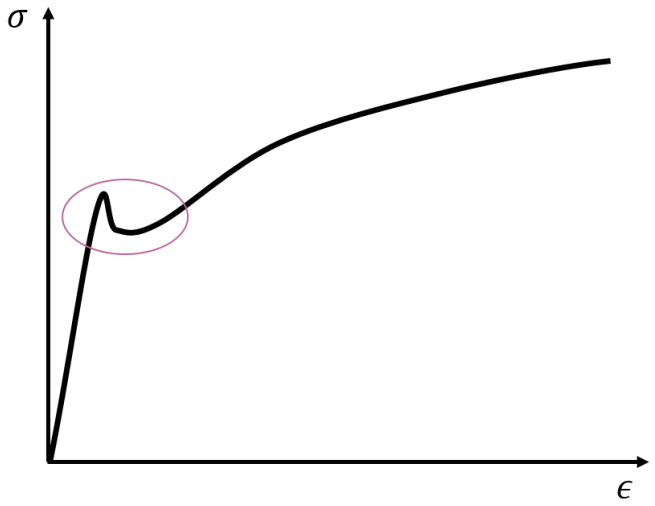

Figure 2.1: Representation of yield drop and plateau in a stress-strain curve.

This disruption in an otherwise smooth curve creates difficulties when fitting parameters to many conventionally used material models, as these models often have

a well-defined or smooth transition between elastic and plastic behavior. The occurrence of Lüder bands introduces further challenges as most experimental measurement techniques provide an average of the specimen deformation which does not capture the local nature of the plastic deformations. The local deformations create further difficulties as the phenomenon may appear more frequently for higher rates of loading.

2.3 Wave propagation in metals

In high strain rate testing, especially in methods like SHPB, understanding wave propagation is important while analyzing the stress and strain distributions. In SHPB testing, both elastic and plastic waves may appear.

Elastic waves in thin bars

When a dynamic force is applied at the end of a bar, it generates a compressive stress wave that propagates along its length. If the length of the bar is large compared to its diameter, the wave can be approximated as a uniaxial stress wave, meaning the stress and strain are primarily along the axis of the bar.

This stress wave propagates at a specific velocity, as each atom in motion transfers its momentum to neighboring atoms, generating the wave motion. The wave velocity, denoted C_0, depends on the material's properties and is described by Equation (2.1), where E is the Young's modulus, representing the stiffness of the material, and ρ is its density [9]:

$$C_0 = \sqrt{\frac{E}{\rho}} \tag{2.1}$$

The relationship shows that the wave speed increases with increasing stiffness or reducing density. Hence, the highest wave speed is obtained in materials with high stiffness and low density.

Plastic waves in test specimens

In SHPB tests an elastic compressive wave travels through a bar, and when it reaches the specimen it partly reflects back as a tensile wave, while the rest travels through the the specimen causing plastic deformation. Therefore, the impedance of the bar and the specimen should match to minimize the reflection of the wave at the transition to ensure sufficient deformation in the specimen.

Due to the SHPB setup, as later described in Chapter 3, the stress in the specimen can be considered uniformly distributed. This uniformity occurs because the wave length of the applied load is longer than the specimen itself, allowing the entire specimen to experience the load wave simultaneously before unloading begins. Consequently, the specimen does not experience a classic plastic wave propagation, as the load affects it uniformly across its length during the loading interval.

At quasi-static or slower dynamic strain rates, the stress waves have a lot of time to travel through the specimen and reflect, and the resulting stress can be assumed one dimensional. As the strain rate increase to what is achieved in SHPB testing, the wave velocity can decrease significantly due to the plastic deformation occurring, which would disturb the force equilibrium assumption. This disruption may be avoided by limiting the maximum allowable impact velocity [10]. The expression for maximum velocity is found in Equation (2.2) [10], using s and b as indices referring to specimen and bar properties. In the equation ρ is the density, c the sound velocity and σ_y is the specimen yield strength.

$$V \leq \left(\frac{\rho_b c_b}{2\rho_s c_s} + \frac{d_s^2}{d_b^2} \right) \frac{2\sigma_y}{\rho_b c_b} \tag{2.2}$$

While interpreting the results from SHPB, assumptions about the wave behavior are required, which can to a certain degree, affect the measurement interpretations. However, the uniform stress distribution assumption is generally needed during data analysis.

2.4 Johnson-Cook Material model

The Johnson-Cook (JC) material model is one of the most commonly used models to predict failure initiation and plastic material behavior. The JC model is used to predict the material behaviour during both low and high strain rates in materials experiencing plastic deformation [11].

The flow stress is defined as the stress required to continue to deform the material plastically at any given moment [12]. The JC parameters are a part of the JC flow stress model, which is expressed as [11]:

$$\sigma_f = (A + B\varepsilon^n) \left(1 + C \ln \frac{\dot{\varepsilon}}{\dot{\varepsilon}_0} \right) \left(1 - \left(\frac{T - T_0}{T_m - T_0} \right)^m \right) \tag{2.3}$$

where, σ_f is the flow stress, ε and $\dot{\varepsilon}$ is the strain and strain rate while ε_0 is the reference strain rate. The parameters T_0, T_m and m are considered known parameters and represents environment temperature, melting temperature and effect of thermal softening [13]. The JC parameters A, B, n and C are described in Table 2.1.

Table 2.1: Description of relevant parameters in the JC model.

Parameter	Description
A	yield stress in the material at reference strain rate.
B	Strain hardening constant at reference strain rate.
n	Strain hardening coefficient at reference strain rate.
C	Strain rate strengthening factor

The JC model could result in a curve as the one in Figure 2.2, where A represents where the red line starts at zero plastic strain and an increased flow stress is observed for increased plastic strain.

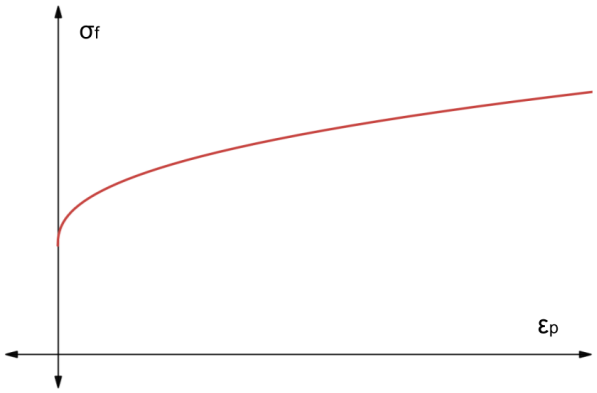

Figure 2.2: Example curve from the JC model equation.

In this thesis, one objective is to find suitable values for the constants A, B, n, and C for a defined reference strain rate.

The temperature related variables are for A36 steel defined as $T_0 = 300$ K, $T_m = 1703$ K and $m = 0.917$ according to [14]. Knowing the JC models limitations in capturing effects like yield drop, this study aims to find a parameter set that still accurately models A36 during different strain rates.

3

Theory of material testing using the Split Hopkinson Pressure Bar

The Split Hopkinson pressure bar (SHPB) setup mainly consists of three bars: the striker, the incident bar and the transmitting bar, which can be seen in Figure 3.1 from left to right. The incident and transmitting bars are long and made from a material with higher strength than the specimen to avoid that they are damaged during testing. The bars are also chosen to have a matching impedance to the specimen to ensure proper wave transmission between them. The specimen is placed between the two bars. The striker bar is made of the same material as the incident and transmitting bars, but has a shorter length. The striker is launched at the incident bar which generates a wave that propagates through the test setup. Strain gauges are placed at an equal distance from the specimen on both the incident and transmitting bar and measures the propagating wave.

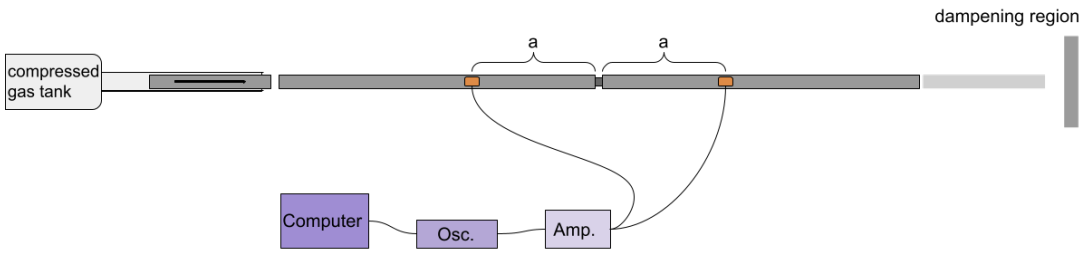

Figure 3.1: Schematic representation of the SHPB setup.

The SHPB ideally deforms the specimen uniformly in combination with achieving high strain rates.

Different parts of the setup is referred to using the indices in the list below, with x being a changeable variable.

index	Definition
x_{str}	striker
x_I	incident bar
x_i	incident wave
x_T	transmitting bar
x_t	transmitted wave
x_s	specimen
x_b	bar, valid for both incident and transmitted

The striker is launched through a tube and impacts the incident bar, which introduces a pressure wave propagating with the speed of sound in the incident bar. The wave is measured by the installed strain gauge and the output voltage can be converted to strain with a scale factor depending on the kind of strain gauge used. The strain in the incident bar is denoted as ε_I. The pressure wave then progates through the specimen and through the transmitting bar where the other strain gauge measures the strain denoted ε_T. When the wave propagates through the surfaces between the bars and specimen reflections occur which are also captured by the strain gauges. This process can also be described through a series of equations [9] [15]. Starting with the wave equation as presented in Equation (3.1):

$$\frac{\partial^2 u}{\partial \tau^2} = c_0 \frac{\partial^2 u}{\partial x^2} \tag{3.1}$$

where u is the uniaxial displacement in the incident bar, τ is time, c_b is the bars speed of sound and x is position in the direction along the length of the bars. Equation (3.1) has a solution on the form in Equation (3.2)

$$u = f(x - c_b\tau) + g(x + c_b\tau) = u_i + u_r \tag{3.2}$$

Physically this equation means that the two functions f and g respectively describe the propagating pulses shape along the x axis in the positive and negative directions [9]. The variables u_i and u_r represent the incident and reflected wave components since we make the assumption of constant wave shapes in the bars [9].

The one dimensional strain is by definition as in Equation (3.3) below.

$$\varepsilon = \frac{\partial u}{\partial x} \tag{3.3}$$

Therefore, Equation (3.2) can be differentiated by x to get the incident bar strain, denoted ε_I expressed as the sum of the incident wave strain and reflected wave strain as in Equation (3.4).

$$\varepsilon_I = \varepsilon_i + \varepsilon_r \tag{3.4}$$

Using the same method for the transmitting bar the strain $\varepsilon_T = \varepsilon_t$, as there is no wave traveling in the negative direction during the observed span of time, the transmitting bar strain is the same as the incident wave strain.

Taking the derivative of Equation (3.2) again and using Equation (3.4), Equation (3.5) is obtained for the incident bar:

$$\frac{\partial u_I}{\partial \tau} = \dot{u}_I = c_b(-\varepsilon_i + \varepsilon_r) \tag{3.5}$$

where u_I is the displacement at the interface between the incident bar and specimen. Similarly Equation (3.6) is obtained for the transmitting bar:

$$\frac{\partial u_T}{\partial \tau} = \dot{u}_T = -c_b\varepsilon_t \tag{3.6}$$

where u_T is the displacement at the interface between the transmitting bar and specimen.

Using the velocities in Equation (3.5) and (3.6) together with the length of the specimen l_s, the strain rate, $\dot{\varepsilon}_s$, in the specimen is expressed in Equation (3.7).

$$\dot{\varepsilon}_s = \frac{(\dot{u}_I - \dot{u}_T)}{l_s} = (-\varepsilon_i + \varepsilon_r + \varepsilon_t)\frac{c_b}{l_s} \tag{3.7}$$

By integration of the previous equation over time, the specimen strain is obtained as in Equation (3.8).

$$\varepsilon_s = c_b \int_0^\tau (-\varepsilon_i + \varepsilon_r + \varepsilon_t)\frac{1}{l_s} d\tau \tag{3.8}$$

Even though this equation is correct, it is not very useful in this SHPB setup since there is no separate measurement of the specimen length during testing, therefore the engineering strain, $\varepsilon_{s,eng}$, in the specimen is expressed instead by using the initial specimen length as seen in Equation (3.9):

$$\varepsilon_{s,eng} = e_s = \frac{c_b}{l_0} \int_0^\tau (-\varepsilon_i + \varepsilon_r + \varepsilon_t) d\tau \tag{3.9}$$

Under uniaxial compression, the true strain, ε_{true}, can be calculated from the engineering strain as Equation (3.10):

$$\varepsilon_{true} = ln(1 + e_s) \tag{3.10}$$

By taking the time derivative of true strain, the true strain rate, $\dot{\varepsilon}_{true}$, is obtained as in Equation (3.11):

$$\dot{\varepsilon}_{true} = \frac{\dot{e}_s}{1 + e_s} \tag{3.11}$$

Besides the strain, the stress in the specimen is also of relevance. Now the assumption of the specimen being in equilibrium is made, starting from the basic expression for stress in Equation (3.12) which is expressed through the forces F_I and F_T acting upon the interfaces between the incident and transmitting bar and the specimen cross section area A_s.

$$\sigma = \frac{F}{A} = \frac{F_I + F_T}{2A_s} \tag{3.12}$$

The forces in the equation above can be expressed with the bars' elastic modulus E_b and cross section area A_b as Equation (3.13) and (3.14) below.

$$F_I = A_b E_b(\varepsilon_i + \varepsilon_r) \tag{3.13}$$

$$F_T = A_b E_b \varepsilon_t \tag{3.14}$$

Inserting Equations (3.13) and (3.14) into Equation (3.12), the specimen stress is obtained and due to the equilibrium assumption F_I is equal to F_T, the expression for stress becomes as shown in Equation (3.15).

$$\sigma_s = \frac{E_b A_b}{A_s}\varepsilon_t \tag{3.15}$$

where ε_T is replaced by $(\varepsilon_i + \varepsilon_r)$. If A_s is handled as the true cross-section area the same issue arise as with the strain, there are no dynamic measurements of the specimen in the setup, hence additional assumptions are required. If the material in the specimen can be assumed incompressible, the true stress can also be expressed in terms of the engineering strain in Equation (3.9):

$$\sigma_{true} = \frac{F}{A_0}(1 + e_s) = \sigma_{eng}(1 + e_s) \tag{3.16}$$

The equations presented in this chapter will be used while processing the data from the performed experiments. Now with the theoretical stress and strain equations established, the next section specifies the the measurement techniques used to collect data during testing.

3.1 Measuring techniques in the Split Hopkinson Pressure Bar

To measure both the incident and transmitting bar strain, a full bridge strain gauge configuration can be used. This allows tension to be measured independently of bending while also compensating for temperature changes. The full bridge consists of four active strain gauges with two pairs rotated by 90° in regards to each other and are coupled as shown in Figure 3.2. While installing, the two pairs of strain gauges are placed on opposite sides of the bar at the same lengthwise location.

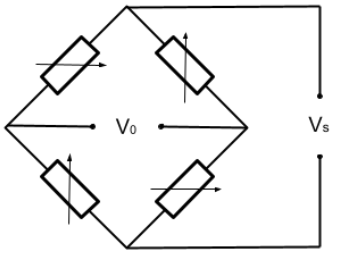

Figure 3.2: Full Wheatstone bridge circuit. Strain gauges are shown as variable resistors with V_s being the excitation voltage and V_0 the output voltage.

Due to there being four strain gauges there is a high output signal giving good resolution in the measuring data. Using the full bridge, the output voltage V_0 is converted to the nominal strain ε by Equation (3.17). In the strain equation, ν is the Poisson's ratio of the bar, k the gaugefactor and V_s the excitation voltage.

$$\varepsilon = \frac{1}{(1+\nu)} \frac{2}{k} \frac{V_0}{V_s} \tag{3.17}$$

As an alternative a half bridge strain gauge configuration can be used instead of the full bridge. The half bridge consists of two active strain gauges rotated 90° from each other and are coupled as in Figure 3.3.

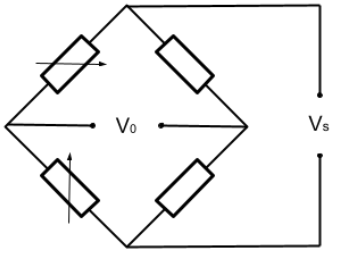

Figure 3.3: Half Wheatstone bridge circuit. Strain gauges are shown as variable resistors with V_s being the excitation voltage and V_0 the output voltage.

The half bridge is temperature compensated for isotropic materials, which usually is a fair assumption for steel materials, including maraging steel if it has not previously been subjected to plastic work [16] [17]. The half bridge has a disadvantage compared to the full bridge in the sense of the output voltage being smaller and bending not being compensated for according to [18]. On the contrary, the installation process is less prone to errors, since strain gauges are sensitive to the adhesive method and easily misaligned. For the half bridge, there is a similar conversion equation from voltage to strain, as shown in Equation (3.18) [18].

$$\varepsilon = \frac{1}{(1+\nu)} \frac{4}{k} \frac{V_0}{V_s} \tag{3.18}$$

4

Experimental setup and test procedures

Both Split Hopkinson Pressure Bar (SHPB) and compression tests in quasi-static and dynamic strain rates were performed during the experimental testing. All specimens were of the same steel quality, A36, cut into small cylinders having both length and diameter of 6 mm. In this chapter, the used experimental setups are described in addition to a description of the optimization method used to obtain the material parameter values.

4.1 MTS compression testing

The slower compressive tests were performed with strain rates of quasi-static $1.6 \cdot 10^{-4}$ 1/s and dynamic 1.25 1/s to cover both quasi-static and slower dynamic strain rates which provide a baseline for the material response under varying loading rates.

The compressive testing for the lower strain rates were preformed using the MTS model 204.31 [19]. The setup was completed with a separate displacement gauge, also from MTS, model 632.06C-22 calibrated to measure displacement. The output options utilized from the MTS machine was: time (s), axial force (N), axial displacement (mm).

The reason for using the additional displacement gauge is because the MTS-machine cannot compensate for eventual flexibility in the machine parts, it only measures in terms of the hydraulic output.

The displacement gauge was mounted on the surfaces which are to be in contact with the specimen during testing as seen in Figure 4.1.

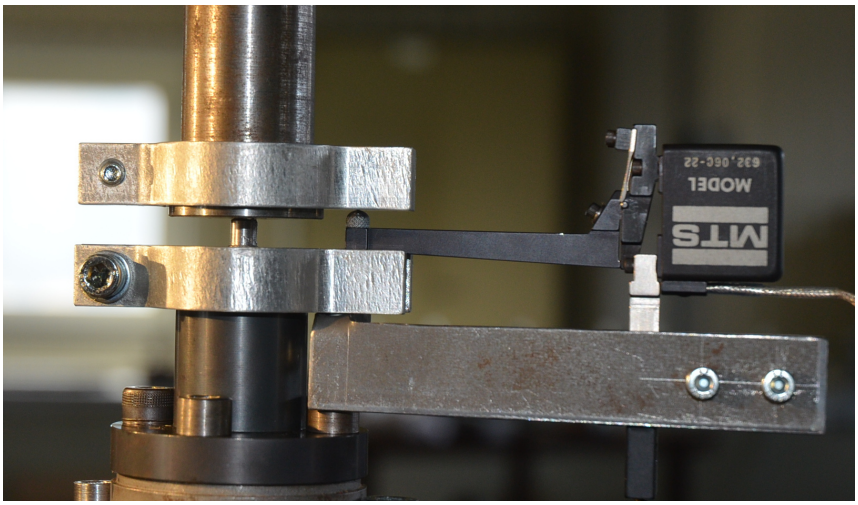

Figure 4.1: MTS setup with displacement gauge and specimen.

4.2 Split Hopkinson pressure bar tests

4.2.1 Setup of the Split Hopkinson Pressure Bar

The striker, incident bar and transmitting bar are all made from the same material, a high strength maraging steel called Vascomax 350. Maraging steel is used because of its high strength to ensure that plastic deformation does not occur in these during the tests. Table 4.1 [20], features the properties of the bars used in the analysis. The dimensions of the bars used are given in Table 4.2.

Table 4.1: VASCOMAX 350 properties.

Property	Description	Value
E	Young's modulus	190 GPa
ρ	Density	8200 $\frac{\text{kg}}{\text{m}^3}$
ν	Poisson's ratio	0.3

Table 4.2: Dimension of bars in the SHPB setup.

Bar	Length (m)	Diameter (mm)
Striker	0.2	12.4
Incident bar	1.892	12.4
Transmitting bar	1.688	12.4

Between the striker and incident bar, a small thin copper disc was positioned to act as minor damping to the pulse to create a nondisperive stresswave [21], and to prevent damage in the bars. This disc is called a pulse shaper. There have been studies about the pulse shapers impact on the results depending on its size and material, but the results are not conclusive and some trial and error is therefore required.

The properties of this setup can be used in Equation (2.2) to get the maximum impact velocity for the striker to assure uniaxial stress in the specimen. This gives a theoretical maximum velocity for this setup of only about 10 m/s, which is exceeded during testing.

The setup is seen from both the front and the back in Figure 4.2, and a specimen placed between the incident bar and transmitting bar is seen in Figure 4.3.

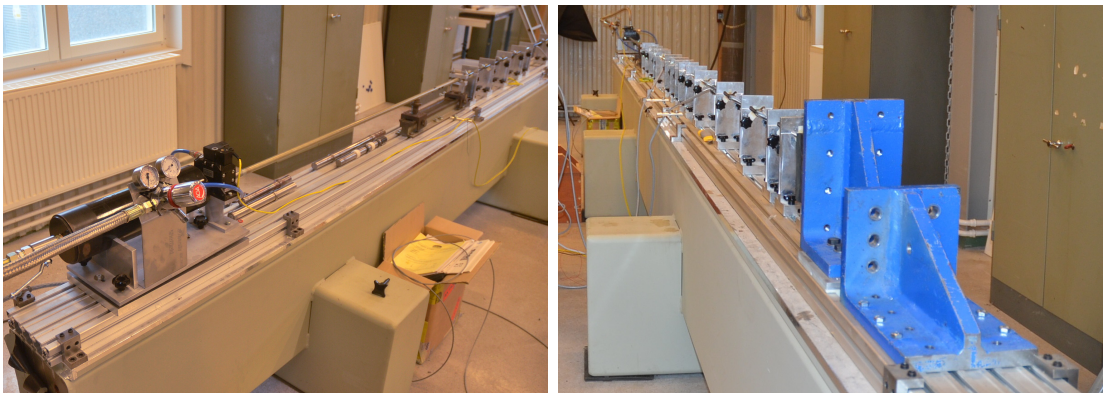

(a) **(b)**

Figure 4.2: (a) Gas tank and barrel in the SHPB setup. (b) Track and support in the SHPB setup seen from the back.

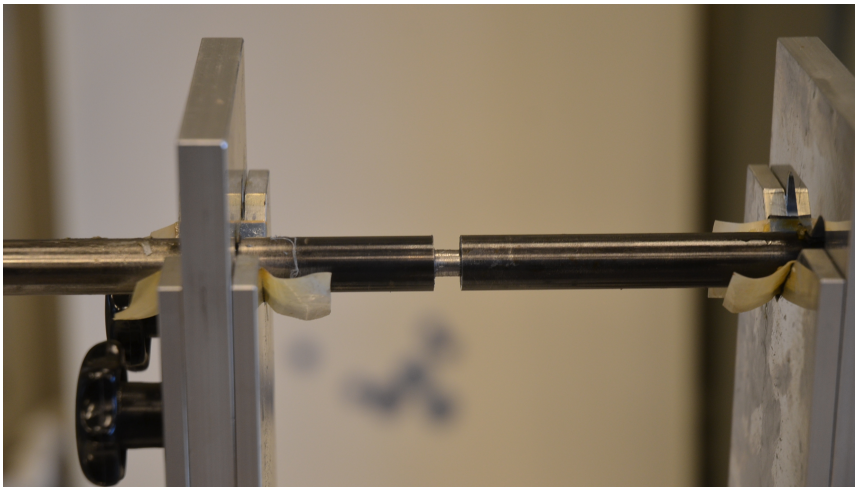

Figure 4.3: Specimen between the incident bar and transmitting bar.

4.2.2 Measurement equipment

The only variable input parameter is the pressure in the gas tank launching the striker, which varied between 5 and 10 bar, mainly focusing on 5 and 7.5 bar. The setup was at first installed with two full bridge configurations, one on the incident bar and one on the transmitting bar. Due to failure in the incident bar strain gauge configuration in test four, a new half-bridge configuration was installed on

the incident bar. This setup was used to collect measurement data from test four and later. The two different strain gauge setups can be seen in Figures 4.4a and 4.4b.

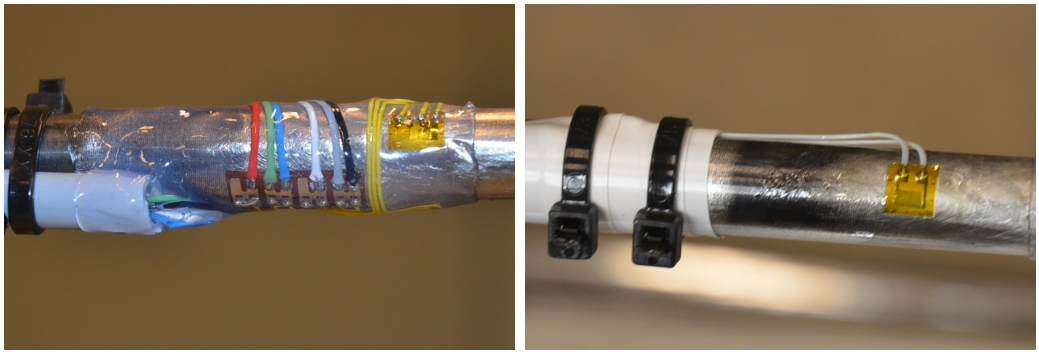

(a) **(b)**

Figure 4.4: (a) One side of the full bridge strain gauge setup. (b) One side of the half bridge strain gauge setup.

The change in strain gauge setup affects the measurement accuracy. However, only minor differences were seen between the tests using different strain gauge configurations.

5

Numerical modeling of material testing

The numerical models enable a more detailed comparison to the experimental tests and serve as a basis for the material parameter optimization. The models were built in LS-DYNA version 14.1.0 [22], which is a multiphysics simulation software suitable for material deformation simulations.

5.1 Compression test model

The model was built to resemble the test conditions used in the hydraulic compressive testing. It consists of two discs and the specimen placed in-between as seen in Figure 5.1.

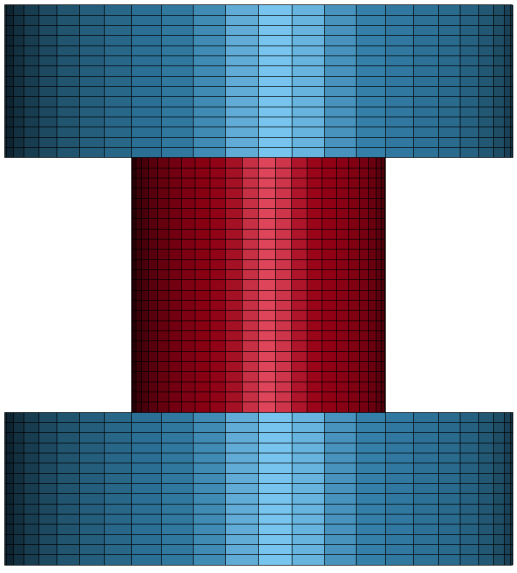

Figure 5.1: Numerical model of the hydraulic compressive testing.

Boundary conditions were introduced on one of the discs to prevent displacement while the other disc was prescribed a displacement velocity matching the experimental test data. The specimen was modeled as a cylinder with a diameter and length of 6 mm. The specimen was modeled with second order elements with a side length

of about 0.3 mm which was determined by a mesh convergence study. The specimen was modeled using the Johnson-Cook (JC) material model and the Grüneisen equation of state with the parameters in Table 5.1. The Grüneisen equation of state defines equations for the compressed and expanded material pressure, dependent on the material density, particle velocities and internal energy [23]. This equation of state is specifically used for materials experiencing shock. These specific parameter values were chosen since these numbers have appeared in previous work done on A36 steel in very high strain rate applications [24]. The two discs were modeled as a stiff elastic material to prevent them from deforming as much as possible. To be able to perform the parameter optimization and results comparison, the specimen force and cross-section dimensions were specified as output data.

Table 5.1: Grüneisen parameters for A36 steel [24].

Grüneisen parameter	Value
C	4569 m/s
S1	1.49
GAMMA0	2.17

The model uses 8-point hexahedron elements together with the hourglass energy type Flanagan-Belytschko for solid elements to prevent the hourglass phenomenon.
Two model variations were run to replicate the compression tests, one quasi-static with a strain rate of $1.6 \cdot 10^{-4}$ 1/s and one dynamic with a strain rate of 1.25 1/s. These were run with explicit time stepping and mass scaling to keep a reasonable runtime.
These models were used in LS-OPT to obtain the material parameters for the JC material model, and the presumed known parameters had the values presented in Table 5.2 [14].

Table 5.2: Material parameters for A36 [14].

Parameter	Value
ρ	7850 kg/m^3
E	210 GPa
ν	0.26

5.2 Split Hopkinson Pressure Bar model

The SHPB model complements the experimental test by validating the JC parameters obtained from LS-OPT. To represent the SHPB experiments, the LS-DYNA model includes the specimen and three bars with equal radius, the incident, transmitting, and striker bar, all with the dimensions in Table 5.3. Part of the model can be seen in Figure 5.2.

Table 5.3: Part dimensions of the SHBP model, which are as close as possible to the experimental setup.

Part	Size
incident bar length	1.98 m
transmitting bar length	1.69 m
striker length	0.2 m
bar diameter	12.4 mm
specimen length	6 mm
specimen diameter	6 mm

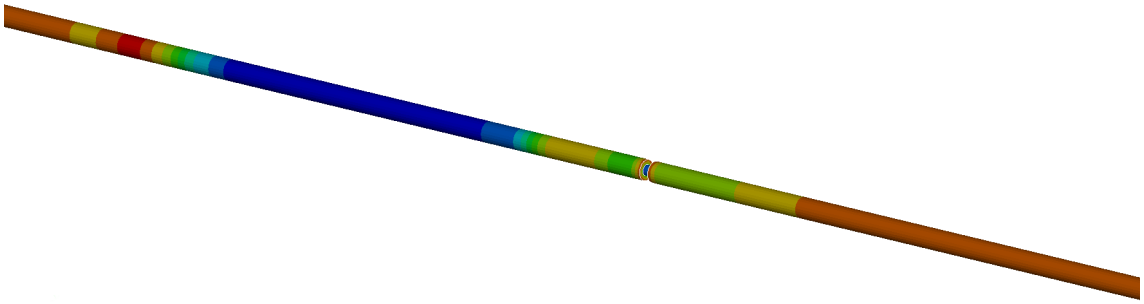

Figure 5.2: SHPB model with incoming stress wave traveling to the right where blue represents pressure and red is unaffected material.

All parts except the specimen were restricted to only have one degree of freedom so that they were free to move in the length direction. The bars were modeled as elastic, since they do not deform plastically, with the material parameters in Table 4.1. Again, the specimen uses the Grüneisen equation of state with the same parameters as the quasi-static model. The SHPB model also uses an explicit time integration scheme but does not use mass scaling as it is not needed or suitable for models with significant dynamic effects.

To get the desired output, displacements were extracted both for the specimen at different positions and at the experimental placement of the strain gauges, to be able to resemble the strain gauge data.

To evaluate the performance of the model, each experimental test was matched to a striker velocity by comparing the strain amplitude in the incident bar. How the model and experimental data are compared will be presented as results in the following chapter.

5.3 Material parameter optimization

LS-OPT is an optimization and analysis software developed by LST LLC which is highly compatible with LS-DYNA models [25], the version used was LS-OPT 7.0.2.

Two different setups were used in LS-OPT to determine the material parameters for the JC model described in Section 2.4. The quasi-static model provides values for A, B and n as these should not be affected by dynamic effects. The dynamic model provides a value for C i.e. the strain rate dependence.

The process in LS-OPT was defined as a Metamodel-based optimization consisting of different stages: sampling, running stage, metamodels, composites, optimization, termination criteria, domain reduction and finally verification. Their flow chart is visualised in Figure 5.3 and the stages are described in more detail below.

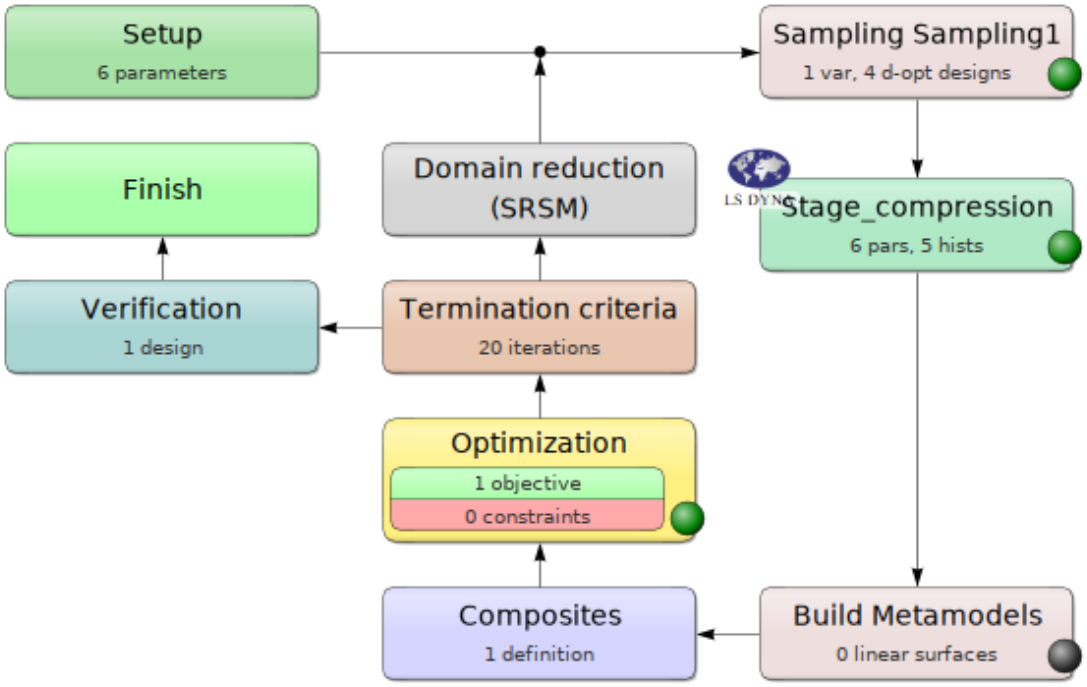

Figure 5.3: LS-OPT flow chart for the dynamic compression tests.

In the sampling and running stage, the number of models to run per iteration is determined before start, along with the parameter values for each iteration. In Figure 5.3, six parameters are indicated but five of them are kept constant and the one active variable can be seen in the sampling stage. The output data needed from the numerical model is defined in the optimization stage. In both the quasi-static and dynamic models, the cross-section force and specimen height were defined as output variables. Due to the varying number of optimized parameters, the model based on the quasi-static compression test runs seven simulations in each iteration to determine the JC parameters A, B and n, while the model of the dynamic compression test runs four simulations in each iteration to determine the JC parameter c.

In the composites and optimization stage, the output from the numerical model is composed into a force-displacement graph. The graph is compared to the experimental data using the mean square error method which is integrated in LS-OPT. The results are evaluated by an Adaptive Simulated Annealing algorithm. To reduce computational time and minimize the impact of local fluctuations, the comparison is made at 100 points along the curves.

The results are then compared to the termination criteria, which is satisfied if the change of parameter values is less than 0.001 and the improvement of the objective function is less than 0.01. If the termination criteria is not satisfied, the domain reduction stage provides a new set of parameter values, and the above described process repeats until the criteria are satisfied.

Since the JC material model cannot fully describe the behavior of A36 steel, particularly the transition zone between elastic and plastic behavior, the measurement data was slightly modified to appear smoother in the transition zone to reduce its influence in the evaluation stage. The data was modified by applying a Gaussian smoothing filter until no extreme peaks or dips were present, which greatly reduced the higher yield point. The modified and original data for both the quasi-static and the dynamic conditions are seen in Figure 5.4 and Figure 5.5 respectively.

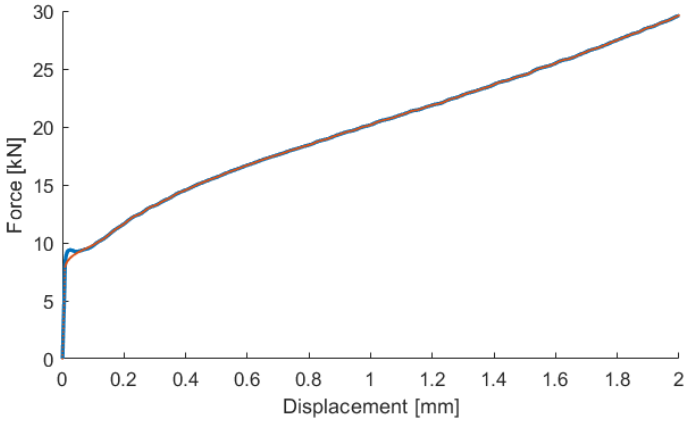

Figure 5.4: Unfiltered data from quasi-static testing in blue and filtered data for use in LS-OPT in red.

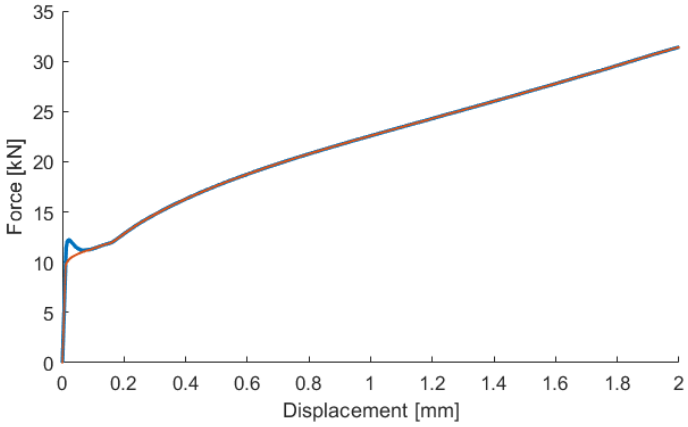

Figure 5.5: Unfiltered data from dynamic testing in blue and filtered data for use in LS-OPT in red.

Together with the measured data from quasi-static testing, the LS-OPT model can determine values for A, B, and n in the Johnson-Cook material model. It was prioritized to fit strains over 0.018 to reduce the impact from the fully elastic region in case of any deviations. To obtain the value for C, the already optimized values of A, B and n from the quasi-static model were fixed, while C was introduced as the only variable parameter. The target curve was changed according to the dynamic experimental data with the same type of filtering as presented earlier.

6
Results

The experimental data obtained were processed by using the equations in Chapter 3. The experimental results were then used as both the base of the LS-OPT optimization and to compare the results to the numerical LS-DYNA models. This chapter shows how the results from the numerical model with the optimized Johnson-Cook parameters from LS-OPT fit the experimental test results both for the hydraulic compression tests and the SHPB tests. It also presents how the physical and simulated specimens are compared and how the data is analyzed.

6.1 Parameter optimization

The optimization algorithm in LS-OPT required eight iterations to reach the convergence criteria. As shown in Figure 6.1, the final iteration of the force-displacement curve for quasi-static conditions fits well with the modified measurement values, except in the area directly following the elastic zone. It is apparent, even in the smoothed curve, that the specimen undergoes a transition between elastic and plastic behavior where the curve temporarily flattens out which cannot be captured by the JC material model.

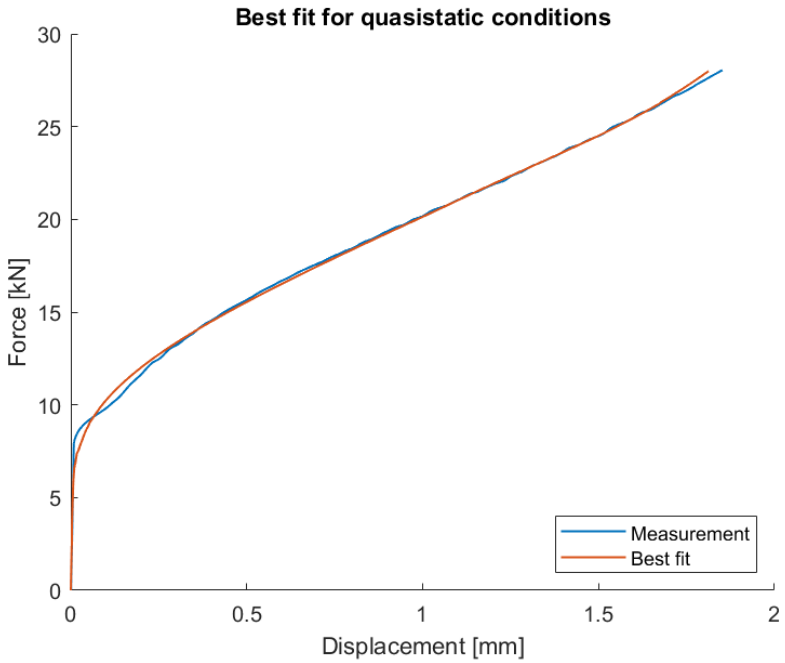

Figure 6.1: The best fitted numerical model compared to the smoothed measurement data for strain rate $1.6 \cdot 10^{-4}$ 1/s.

For the dynamic conditions with strain rate 1.25 1/s, the algorithm required five iterations to reach convergence between the experimental force-displacement data and the simulated data. Looking at the force-displacement curves in Figure 6.2 and comparing it to the quasi-static curves in Figure 6.1, there is a larger difference in the transition zone for the dynamic case compared to the quasi-static. In addition to a overall larger difference throughout the curves while comparing the experimental and simulated data. It looks like the material model response in the plastic region would be able to achieve a better fit if the curve was transferred against larger deformations. There is a slight increase in the modeled applied force right at the end of the curve compared to the measurement data, the same thing can be seen in the quasi-static case but it is not as noticeable.

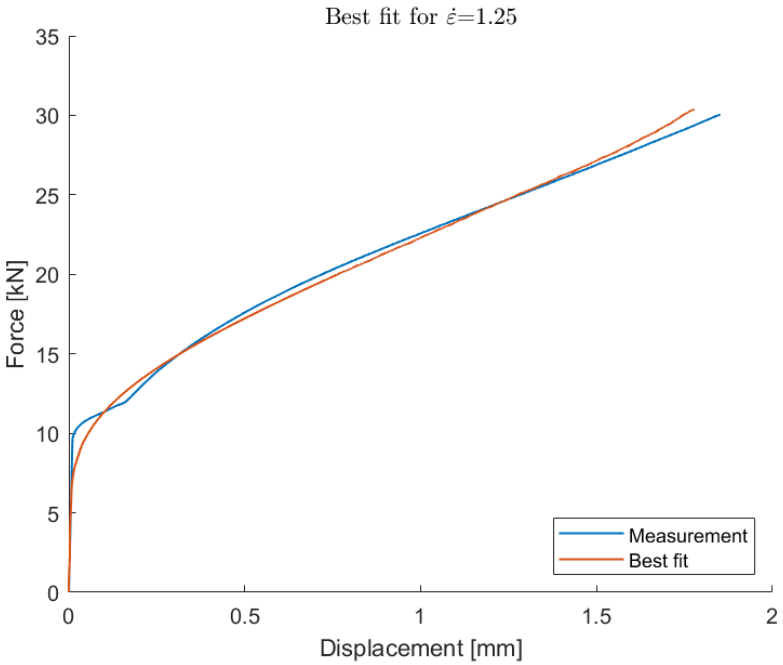

Figure 6.2: The best fitted numerical model compared to the smoothed measurement data for strain rate 1.25 1/s.

The JC parameters extracted from the optimization results in LS-OPT are found in Table 6.1. These are later to be used is the SHPB modeling.

Table 6.1: Johnson-Cook parameters obtained for A36 steel from LS-OPT.

Parameter	Value
A	171 MPa
B	725 MPa
n	0.35
C	0.012

6.2 Material testing

Uniaxial compressive tests

All specimen dimensions were measured before and after testing, the measurements are found in Table 6.2 with their respective strain rate. In the table, L_1 is the specimen length before testing and L_2 the length after compression while D_1 and D_2 is the specimen diameter before respectively after testing measured at the widest point. It should be noted that the amount of compression observed is not representative of the material behavior by itself. A different amount of gap between the top plate and top of the specimen at the start of the test would result in a different amount of final compression.

Table 6.2: Measurements from uniaxial compressive test specimens.

test	L_1 (mm)	L_2 (mm)	D_1 (mm)	$D_{2,mid}$ (mm)	$\dot{\varepsilon}$ (s^{-1})
MTS1	5.96	4.81	5.99	7.71	$1.6{\cdot}10^{-4}$
MTS2	5.98	3.63	6.00	7.83	$1.6{\cdot}10^{-4}$
MTS3	5.98	3.05	5.98	8.55	$1.6{\cdot}10^{-4}$
MTS4	5.97	3.52	5.98	7.92	1.25
MTS5	5.98	3.74	5.99	7.70	1.25

As can be seen in Figure 6.3 and Figure 6.4, the uniaxial compressive test specimens show a varying degree of barreling, meaning an outward rounded protrusion of the sides, which becomes more significant for tests with larger compressive deformation. The specimens appear quite smooth, with no visual additional damage. All results from the uniaxial compression test shows effect from barreling which is caused by the restricting movement at the surfaces caused by friction. It does not appear to be any significant difference between the tests with varying strainrates, see Figure 6.3 and Figure 6.4.

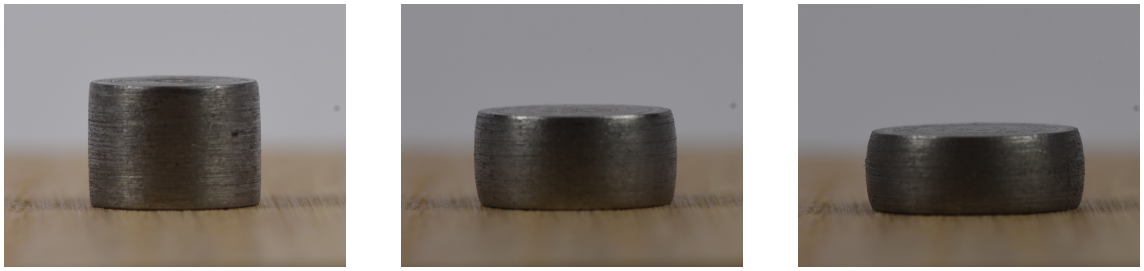

(a) MTS1 **(b)** MTS2 **(c)** MTS3

Figure 6.3: Specimens from uniaxial compressive testing with strain rate $1.6 \cdot 10^{-4}$ 1/s, the difference between a), b), and c) is the amount of compression.

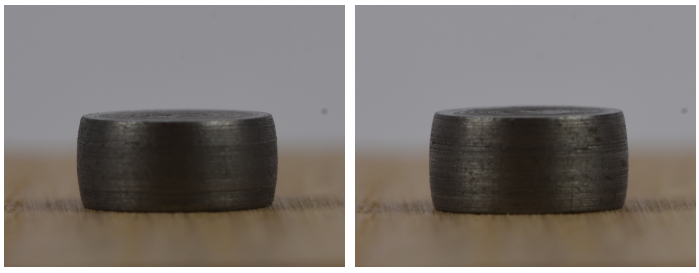

(a) MTS4 **(b)** MTS5

Figure 6.4: Specimens from uniaxial compressive testing with strain rate 1.25 1/s, the difference between a) and b) is the amount of compression.

The stress-strain curve from the uniaxial compressive tests is similar throughout the different tests of the same strain rate, as visualized in Figure 6.5. A significant difference can be seen between the quasi-static and dynamic tests. There is a distinct yield drop in the stress-strain curve, a clear lowering of the yield stress for the

dynamic scenarios, and more of a plateau in the quasi-static tests. Compared to the quasi-static test, the higher yield point exhibited an increase of about 30 % for the dynamic case and an overall increase in yield stress of between 5-10 %.

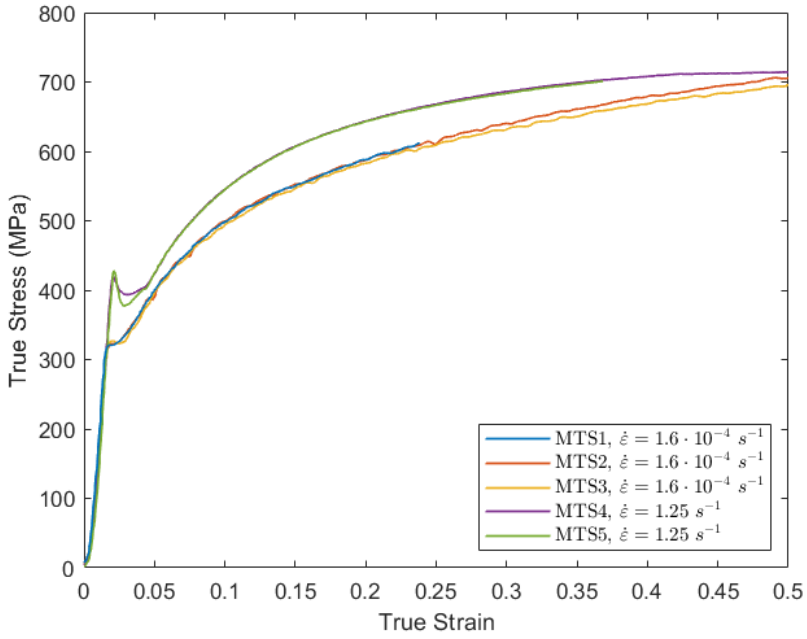

Figure 6.5: True stress against true strain for the uniaxial compressive tests.

To evaluate specimen geometry, the final diameters of the specimens were compared to simulations that had the same final height as in the experimental tests. Except for the least deformed specimen, MTS1, it was found that the simulations consistently predicted a diameter that slightly exceeds the measured and this is presented in Table 6.3.

Table 6.3: Diameter comparison between tests and simulations.

test	measured diameter (mm)	simulated diameter (mm)
MTS1	7.71	6.9
MTS2	7.83	7.9
MTS3	8.55	8.7
MTS4	7.92	8.0
MTS5	7.7	7.8

Height wise, MTS2 and MTS5 were compressed to a similar degree but with different strain rates. In the photographs, Figure 6.3b and Figure 6.4b, appear quite similar. In the LS-DYNA models, a difference can be seen in Figure 6.6, mainly in the region where the widest section appears. The quasi-static MTS2 model is widest in the middle while the dynamic MTS5 model is widest a bit closer to the bottom.

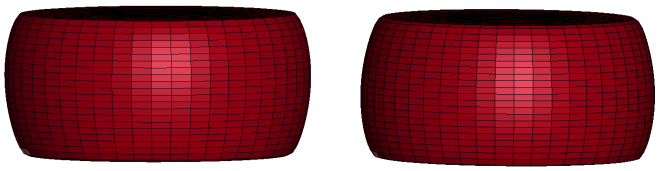

(a) MTS2 **(b)** MTS5

Figure 6.6: Shape of the specimens after compression in LS-DYNA for different strain rates, where some dynamic effects appear present due to the slight shape difference.

Overall, the numerical model of the uniaxial compressive testing preformed adequately. The differences and inconsistencies between the experimental and numerical results will be analyzed in the discussions chapter. Next, the results from SHPB will be examined by evaluating how the numerical model compares to the experimental data.

Split Hopkinson Pressure Bar tests

The SHPB specimen's length and diameter were measured with digital calipers before and after testing, the measurements are found in Table 6.4. In the table again, L_1 is the specimen length before testing and L_2 the length after compression while D_1 and D_2 is the specimen diameter before respectively after testing measured at the widest point. Some of the SHPB specimens showed signs of further damage after testing in the form of indents of different depths, mostly occurring along the corner edges. These indents are probably due to the specimen bouncing around and hitting the sharp edges of the bars after losing contact with the bars. These imprints do not appear to significantly alter the overall shape and are unlikely to have impacted the material behavior. After the tests the specimens generally had almost straight edges, as can be seen in Figure 6.7. They show limited to no signs of barreling compared to the hydraulically compressed specimens. This means there was no significant amount of friction acting upon the specimen and the stress is mostly uniaxial.

Table 6.4: Measurements of SHPB tests where all measured heights are presented in mm. Strain gauge configuration type is given in order for the incident and transmitting bar.

test	L_1	L_2	D_1	$D_{2,mid}$	$\dot{\varepsilon}$ (1/s)	Strain gauge configurations
SHPB1	5.98	5.34	5.99	6.37	1550	full-full
SHPB2	5.98	5.13	5.99	6.52	2100	full-full
SHPB3	5.98	3.8	5.94	7.52	4000	full-full
SHPB4	5.98	4.99	5.97	6.58	2350	full-half
SHPB5	5.98	4.38	5.96	7.14	3300	full-half
SHPB6	5.97	4.51	4.6	6.84	3050	full-half

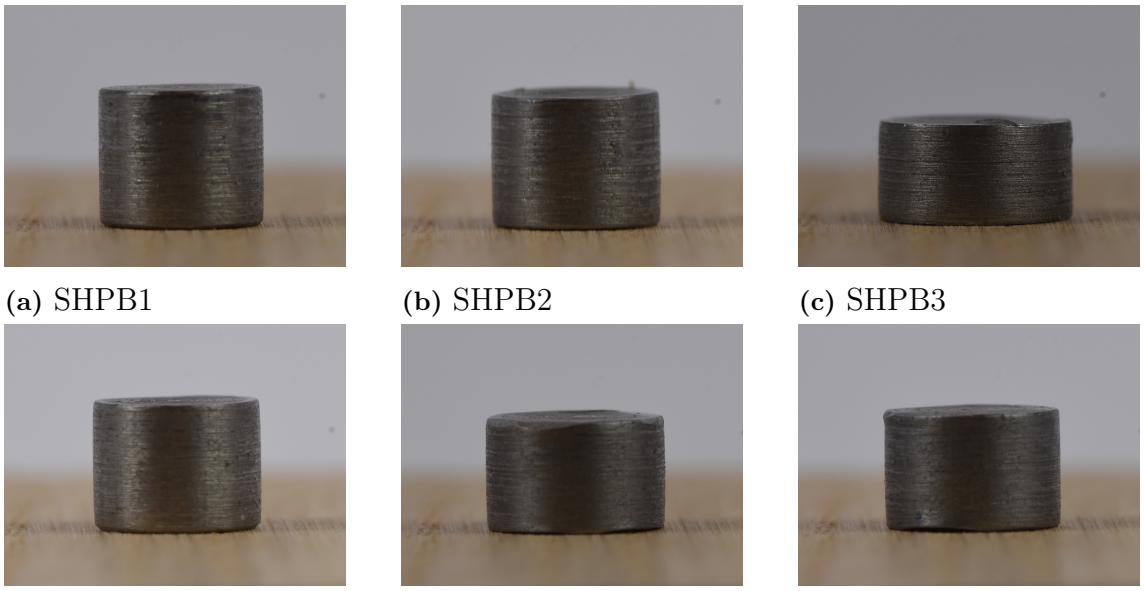

(a) SHPB1 (b) SHPB2 (c) SHPB3

(d) SHPB4 (e) SHPB5 (f) SHPB6

Figure 6.7: Specimens from SHPB testing.

All modeled SHPB specimens have a similar apperance, with varying heights and a slight curvature along the side edge. The modeled shape corresponds well with the physical test specimens. Slight irregularities along the top and bottom edges can be seen in the model specimen in Figure 6.8. In the top right and bottom left corners such irregularities can be seen, they likely appear due to contact issues.

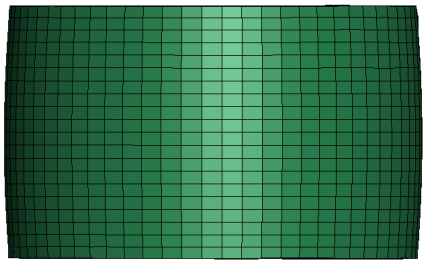

Figure 6.8: LS-DYNA model specimen representing SHPB5.

The SHPB tests and the results from the LS-DYNA model were compared by the final height of the specimens. The physical specimen almost consistently ended up longer than the modeled specimen as can be seen in Table 6.5. SHPB3 is an exception which is of particular interest considering it had the highest input incident bar strain.

Table 6.5: Specimen height comparison between tests and simulations.

test	measured length (mm)	simulated length (mm)
SHPB1	5.34	5.10
SHPB2	5.13	4.85
SHPB3	3.8	3.98
SHPB4	4.99	4.78
SHPB5	4.38	4.30
SHPB6	4.51	4.44

From the measured data, the average true stress and average true strain in each specimen were calculated and plotted together in Figure 6.9. It can be seen that the stress consistently rises with an increased strain rate. After the initial loading, the stress keeps rising slowly until unloading. It is difficult to determine if the yield drop phenomenon is present for the slower rates of loading since measurement errors cause an overshoot from rapid loading. However, an increase in stress level is observed in the SPHB tests compared to the unixaial compressive tests, see Figure 6.5. By comparing stresses at the strain 0.15, the SHPB tests are within the interval 700 to 900 MPa and the MTS test within 550 to 600 MPa, which points to a significant strain rate dependence, especially since the stress levels increase together with the strain rate.

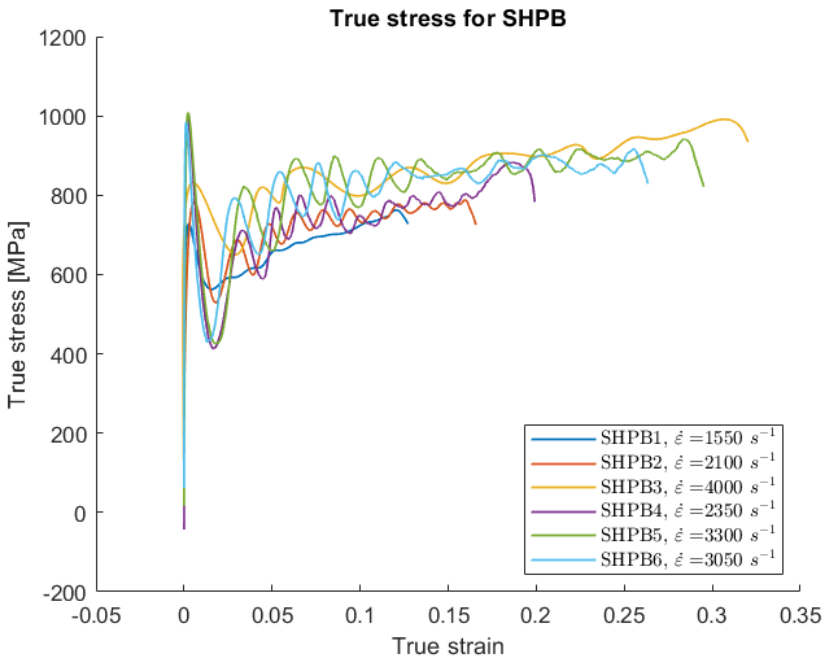

Figure 6.9: True stress-strain plot for the SHPB tests.

To evaluate the fit of the parameters obtained from LS-OPT, the strain measurement data was compared to the corresponding data from the LS-DYNA model, and the specimen sizes were compared. In Figure 6.10 to Figure 6.15, the strain data are compared and it is observed that the incident waves correlate quite well both in

amplitude and in width, especially for tests 4, 5, and 6. The modeled transmitted wave amplitude has a good fit with the measurements for all tests. They have less fluctuations but still follow the average slope. The reflected wave in the incident bar shows quite severe fluctuations and spikes for SHPB tests 1 and 2 and is missing completely for test 3 due to strain gauge malfunction, there is for both of these a peak at the end of the wave not seen in the other tests. In all cases, the amplitude of the reflected wave from the simulations is too high.

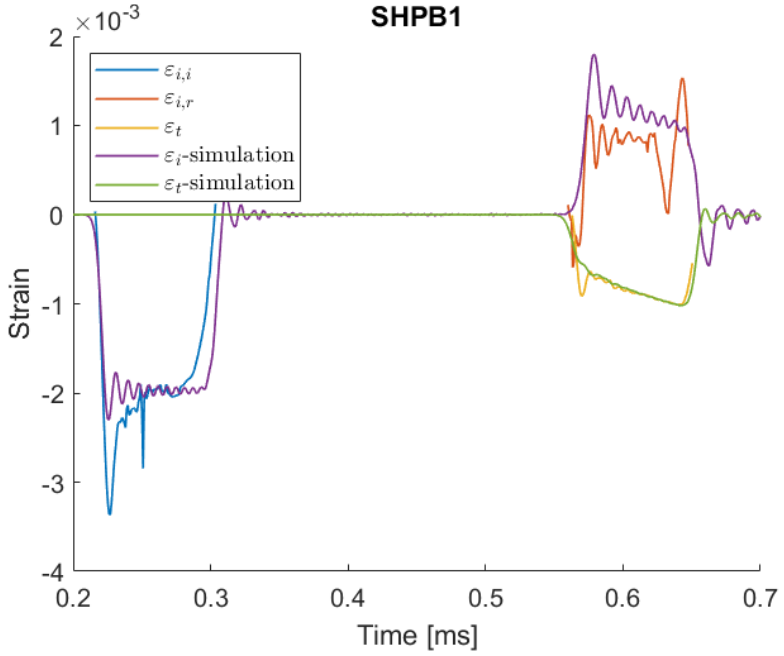

Figure 6.10: Experimental and simulated data from the SHPB1 test.

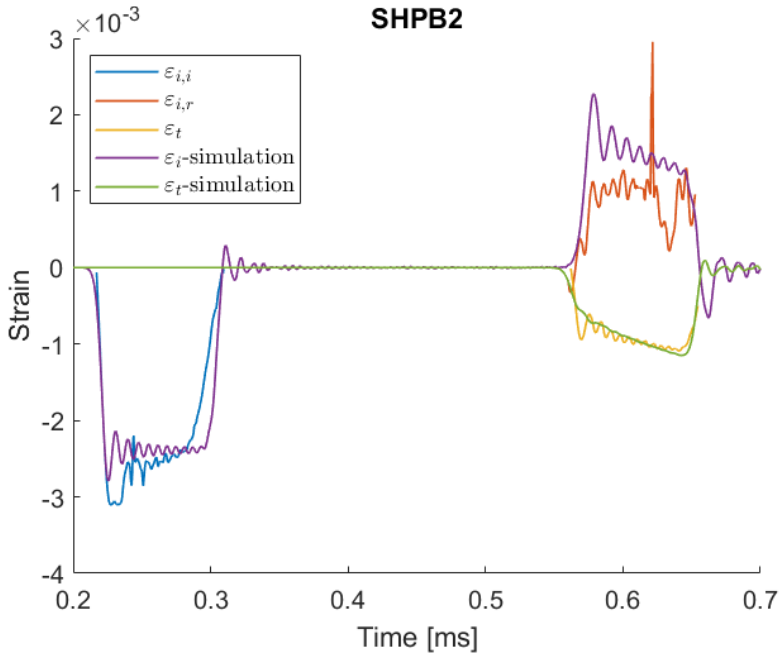

Figure 6.11: Experimental and simulated data from the SHPB2 test.

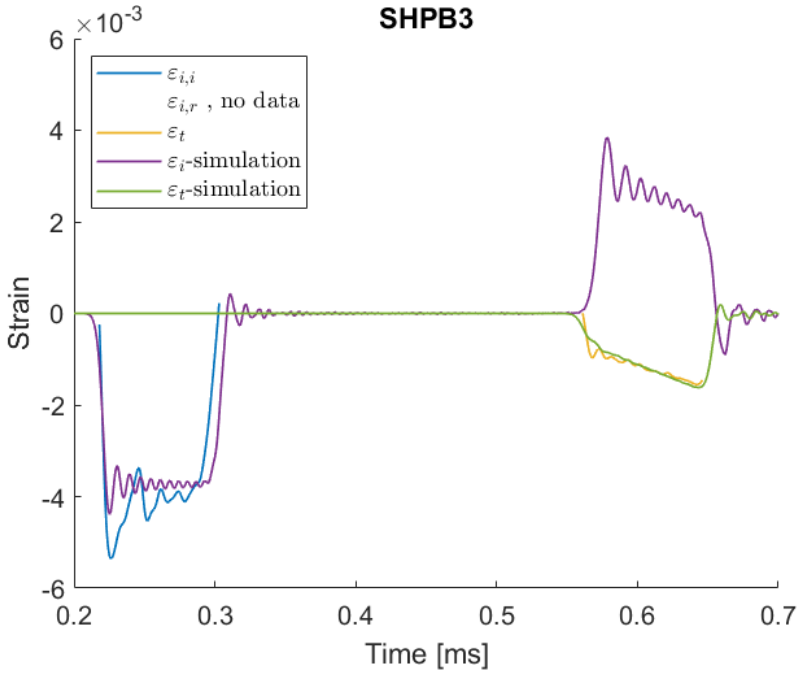

Figure 6.12: Experimental and simulated data from the SHPB3 test.

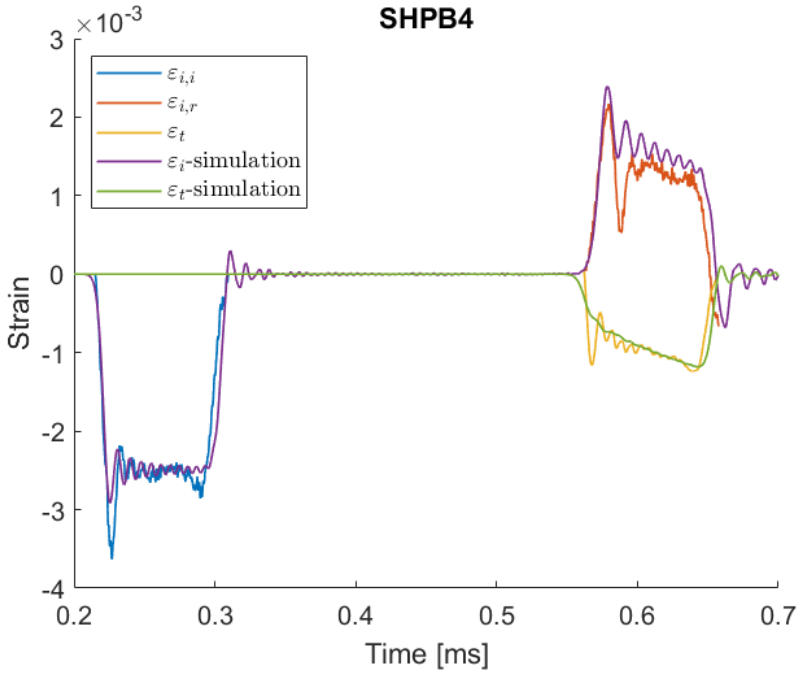

Figure 6.13: Experimental and simulated data from the SHPB4 test.

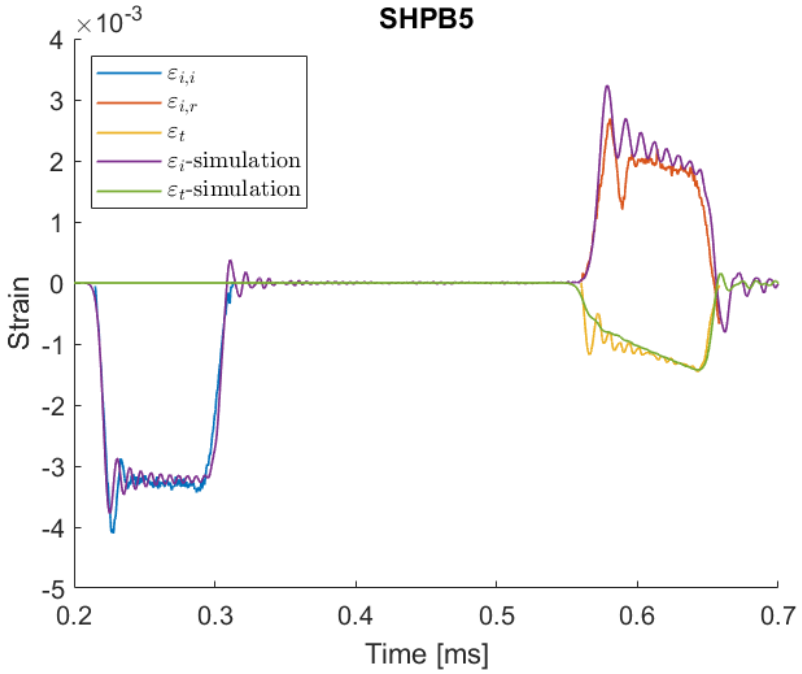

Figure 6.14: Experimental and simulated data from the SHPB5 test.

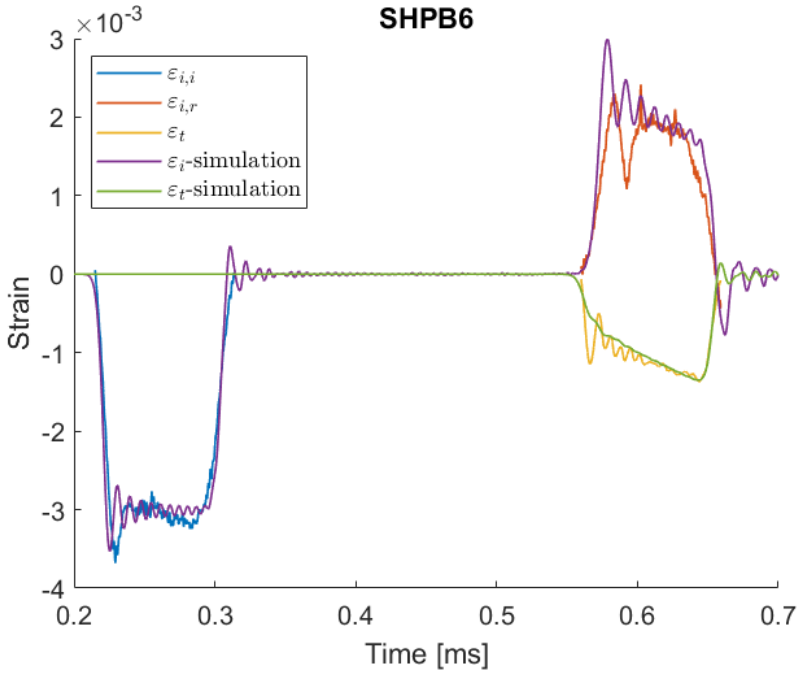

Figure 6.15: Experimental and simulated data from the SHPB6 test.

In summary, these results highlight A36 steels strain rate dependence, and there are prominent deviations from the JC model in the transition zone between elastic and plastic deformation. The same tendencies are seen in all SHPB results, providing consistency and a generally good fit. The results provide a base for further analysis in the upcoming discussion chapter, where the findings and their implications are discussed in more detail.

7
Discussion

This chapter presents a discussion of the comparison between the experiments and the numerical models. It focuses on findings related to wave behavior and how it is affected by the optimized JC parameters. Discussions regarding the experimental setup are addressed where they might have influenced the results as well as being handled separately to bring forward sources of error.

Looking at the parameters obtained from the optimization the value of A=171 MPa, in the JC model, immediately raises some questions as it commonly for steel takes on a tabulated value of 300 MPa or higher when the yield point is defined as the point where 0.2 % plastic strain is obtained. Since metals often show some non-linearity before the expected upper yield point it is reasonable that A would obtain a lower value than first expected from its definition. It is however clear that this is a direct consequence of the non-linearity, yield drop and the transition zone between the elastic and plastic behavior and there is no clear way to handle this while using the JC model. When allowing A to adopt a lower value the model will yield a reasonable result for larger deformations, but one consequence is a smaller elastic deformation range, resulting in more plastic deformation. This becomes more significant in applications where the elastic to plastic region either is observed or happens to lie close to the desired deformation. With this reasoning, the modeled specimens will be a bit shorter in the end, compared to the specimens from the experiments, which is consistent with the obtained results.

For the strain rate sensitivity, which is modeled with the parameter C, it is difficult to determine its accuracy. Changing the value of C would change the amplitudes of both the reflected and transmitted waves. An increase of C would increase the amplitude of the reflected wave and decrease the amplitude of the transmitted wave. From this, it is concluded that there is a slight underestimation of the energy absorbed by the specimen, intuitively this would mean the specimen would not have deformed enough, which is not the case if the previous discussion about the parameter A is true. Again, it is observed that the experimental setup has more loss of energy than the modeled one.

The JC parameters B and n are even more challenging to evaluate as they are largely affected by the value of A. Therefore it is reasonable to believe an improved method of determining A, would provide usable values for the two remaining parameters.

As was shown in the results the comparison between experimental force-displacement

data and simulated force-displacement data from the hydraulic tests showed a higher force towards the end of the range of observed displacement. This could be due to the specimens starting to show significant barreling and geometric effects affecting the stress. Since the observed phenomenon is more prevalent for the dynamic compressive tests, strain rate effects could be involved as the true strain rate of the specimen would increase for the more compressed specimen. As this deviation is present independent of strain rate, it is likely a combination of these reasons and more than likely a modeled specimen specific behavior rather than a modeled material specific behavior.

Looking into the experimental setups and how the results might have been affected by them, there are several aspects to discuss, elastic deformation in the MTS setup, friction at the specimen interface, strain gauge measurements and striker velocity in the SHPB.

The elastic deformations in the hydraulic testing machine mainly affect the early part of the load curve and have minimal impact on the measurements after the initial yield of the specimen. It does however limit the ability to confirm the Young's modulus of the material and would without the additional displacement gauge make the measurement of total displacement less accurate. The displacement measurement should however be sufficiently accurate to not noticeably alter the resulting material parameters.

The variable input in the numerical SHPB model was, as previously described, the striker velocity, which was used to match the incident wave amplitudes since there were no measurements taken of the striker velocity. If the velocity would have been measured the incident wave could be used as a reference as well as to eliminate some uncertainties in the numerical model. The material parameters used to model the bars could then be further evaluated, as well as the transfer of the waves between them.

The specimen and data from the numerical model generally follow the expected behavior in comparison to the experiments. Some deviations between the numerically modeled and experimental results have been noticed and connected to potential causes, which could serve as areas for improvement in future work. As mentioned, the JC parameter A limits the applicability of the parameter set, while the parameter C seems to have been effectuated to a reasonable value, since the increasing strain rate does not affect the fit between the model and experiments.

While comparing the SHPB experiments and the simulated curves, the modeled transmitted wave fits well with the experimental curve through each test. This proves some consistency of the results and acts as reassurance of the selected striker velocities, which were chosen based on the incident wave amplitudes. The simulated transmitted curve exhibits less fluctuations than the measurements, which could either imply a more damping effect in the modeled specimen or that the strain gauges show more fluctuations than what actually exist due to the rapid varia-

tions in strain. Plastic deformation can cause more attenuation of the stress wave, which is consistent with the measured specimen lengths. The deformation of the specimens is almost consistently larger for the simulated specimen compared to the experimental, meaning the simulated transmitted wave could have correctly been more dampened while passing through the specimen. To further compare the fluctuations in the data, looking at the incident waves, the severe fluctuations in the experimental data could be contributed to measuring errors from the strain gauges. Looking at the reflected wave in the incident bar, the large peak at the end of the wave present in tests 1 and 2 strongly suggest some of the equipment in the first full bridge strain gauge setup is contributing to the phenomena. Simultaneously the expected experimental periodic fluctuations are not as easily distinguishable as they are small and hidden among within the noise. The observed fluctuations makes it more difficult to distinguish wave characteristics and leaves larger room for interpretation of differences in wave amplitude, reducing the reliability of the results. Capturing the wave behavior more accurately is necessary to evaluate and model the high strain rate behavior. Fluctuations like those discussed above could lead to incorrect assumptions, causing the wave amplitude to be under or overestimated.

One consistent difference between the experimental and modeled waves are the amplitudes of the reflected waves which are too high in the simulations. The amplitude being too high means too much of the pressure wave was reflected at the interface with the specimen. This is probably due to several causes. Firstly, the numerically modeled contact between the specimen and incident bar is undoubtedly more consistent than in the experiments which may lead to less loss of energy. Secondly it can be an issue with the obtained material parameter values. Too much wave reflection could be due to the impedance difference of the bar and specimen, which could either imply deviations in the assumed material parameters for the bar or the specimen. If it is due to the specimen parameters, it could either be due to the original assumptions of density and Young's modulus or the changes determined by the JC parameters.

As mentioned earlier in the discussion, there are indications of inadequate loss of energy in the numerical model of the SHPB. One probable cause is friction between the bars and their tracks. The bars should ideally slide without friction, but keeping in mind that the incident bar has a small range of motion during the period of specimen deformation, the loss should not be exceedingly large. The numerical model was defined without friction along the bars as it would probably have caused more issues than improvement due to the assumptions and estimations needed. Another cause of energy loss could be the conditions of the tracks supporting the bars. If they are not completely straight or leveled, some bending or misalignment might occur, resulting in energy loss due to the pressure wave propagation or unideal transfer of the wave in the contact area against the specimen.

The fluctuations and inaccuracies in the strain gauge measurements have been discussed, and now their potential sources of error will be covered. As previously mentioned, the gauge configuration affects the accuracy level and self compensating

properties, which would suggest more accurate results for the three first presented SHPB tests, where the full bridge configuration was used. This is however is not reflected in the obtained results, suggesting other disturbances in the setup. Since the strain gauges are sensitive to the installation there is a possibility that some part of the adhesive had failed. Loosening of the adhesive would not necessarily cause fluctuation like the ones observed and is more likely due to sensitivities in the wiring. If the strain measurements could be improved it would open up the possibility of using the SHPB experimental results for the parameter optimization. As for now, it will not be possible to create reasonable curves to use in the optimization process and well motivate the needed filtering.

The setup of the numerical models is considered successful, showing consistency and is well adapted to the experimental behavior. The optimization process appears to perform well. However, it reveals the challenges of modeling a specimen experiencing a yield drop with the JC model. The discussed experimental challenges influenced the results, implying a need for improvements in future work. The discussed findings highlight both the limitations and potentials of combining SHPB testing with material characterization while studying high strain rate behavior.

8

Conclusions

This thesis aimed to combine high strain rate experimental testing and numerical modeling to obtain material parameter values for A36 steel using the JC model. The objectives were focused on evaluating the ability of the method to predict the behavior of A36 steel subjected to loading with different strain rates. This chapter summarizes the findings and their implications and limiting factors.

The untypically low value of parameter A is not consistent with the majority of published work. Due to the nature of the JC model the lower value is not necessarily wrong since it is the combination of all material parameters that is considered, and a low value of A can be counteracted by the other parameters allowing more deformation hardening. For large deformations this can be sufficient, while for observing smaller deformations the error will be comparatively larger. While the JC model succeeded in capturing the strain rate dependence, the limitations are prominent. The limitations could potentially be overcome by changing the optimization reference data to either include other physical properties, or more specifically choosing the range of observed plastic deformation to start closer to the 0.2 % plastic strain from the yield point definition.

The experimental results demonstrated some consistency in the measured strain behavior, but the fluctuations and noise resulted in an inability to fully utilize the data since heavy filtering was difficult to motivate, as discussed in Chapter 7. Improving the strain measurements and introducing direct measurement of the striker velocity would give more reliable data to enable the SHPB experiments to influence the parameter optimizations.

The results in this thesis show both the strengths and limitations of this method, and it demonstrates the possibility of combining numerical models with experimental testing during material characterization. It opens up to further research aimed to improve the reliability of material modelling under dynamic loading condtions.

9
Further research

To achieve a more useful set of parameters for the Johnson-Cook model to describe A36 and other grades of steel under dynamic loading, further research is needed. Based on the observations made during this thesis two suggested areas of improvement are presented here.

The measurement methods during the Split Hopkinson Pressure Bar testing must be improved to provide more consistent and disturbance-free data. Additional measurement of the striker velocity or dynamic measurement of the specimen deformation would provide more data points to be utilized during parameter optimization, however at the cost of simplicity.

From the discussion about the issues of fitting the experimental data to the Johnson-Cook material model it would be of interest to examine alternative models. This would be particularly useful if the model handles the transition from elastic deformation to plastic deformation differently.

Bibliography

[1] Metals USA, "A36 grade structural steel," 2024, https://www.metalsusa.com/a36-grade-structural-steel/ [Accessed: (november 2024)].

[2] W. Chen and B. Song, *Split Hopkinson (Kolsky) Bar: Design, Testing and Applications*. Springer US, 2011. [Online]. Available: http://dx.doi.org/10.1007/978-1-4419-7982-7

[3] R. Davies, "A critical study of the hopkinson pressure bar," *Philosophical Transactions of the Royal Society of London. Series A, Mathematical and Physical Sciences*, vol. 240, no. 821, p. 375–457, Jan. 1948. [Online]. Available: http://dx.doi.org/10.1098/rsta.1948.0001

[4] H. Kolsky, "An investigation of the mechanical properties of materials at very high rates of loading," *Proceedings of the Physical Society. Section B*, vol. 62, no. 11, p. 676–700, Nov. 1949. [Online]. Available: http://dx.doi.org/10.1088/0370-1301/62/11/302

[5] Häfliger, Severin, Fomasi, Sara, and Kaufmann, Walter, "Influence of quasi-static strain rate on the stress-strain characteristics of modern reinforcing bars," *Construction and Building Materials*, 2021. [Online]. Available: http://hdl.handle.net/20.500.11850/476816

[6] E. N. Borodin, A. A. Gruzdkov, A. E. Mayer, and N. S. Selyutina, "Physical nature of strain rate sensitivity of metals and alloys at high strain rates," *Journal of Physics: Conference Series*, vol. 991, p. 012012, Apr. 2018. [Online]. Available: http://dx.doi.org/10.1088/1742-6596/991/1/012012

[7] R. Schwab and V. Ruff, "On the nature of the yield point phenomenon," *Acta Materialia*, vol. 61, no. 5, p. 1798–1808, Mar. 2013. [Online]. Available: http://dx.doi.org/10.1016/j.actamat.2012.12.003

[8] R. Hutanu, L. Clapham, and R. Rogge, "Intergranular strain and texture in steel luders bands," *Acta Materialia*, vol. 53, no. 12, p. 3517–3524, Jul. 2005. [Online]. Available: http://dx.doi.org/10.1016/j.actamat.2005.04.008

[9] M. A. Meyers, *Dynamic Behavior of Materials*. Wiley, Sep. 1994. [Online]. Available: http://dx.doi.org/10.1002/9780470172278

[10] Z. G. Wang and L. W. Meyer, "On the plastic wave propagation along the specimen length in shpb test," *Experimental Mechanics*, vol. 50, no. 7, p.

1061–1074, Oct. 2009. [Online]. Available: http://dx.doi.org/10.1007/s11340-009-9294-x

[11] V. Kumar Reddy Sirigiri, V. Yadav Gudiga, U. Shankar Gattu, G. Suneesh, and K. Mohan Buddaraju, "A review on johnson cook material model," *Materials Today: Proceedings*, vol. 62, p. 3450–3456, 2022. [Online]. Available: http://dx.doi.org/10.1016/j.matpr.2022.04.279

[12] CiteDrive, Inc, "Flow stress," 2023, https://en.wikipedia.org/wiki/Flow_stress [Accessed: (november 2023)].

[13] H. Nam, J. Kim, J. Han, J. Kim, and Y. Kim, *Ductile fracture simulation for A106 Gr.B carbon steel under high strain rate loading condition.* Elsevier, 2014, p. 37–41. [Online]. Available: http://dx.doi.org/10.1533/9780081002254.37

[14] M. Gomah and M. Demiral, "An experimental and numerical investigation of an improved shearing process with different punch characteristics," *Strojniški vestnik – Journal of Mechanical Engineering*, vol. 66, no. 6, p. 375–384, Jun. 2020. [Online]. Available: http://dx.doi.org/10.5545/sv-jme.2020.6583

[15] G. Bodare, "Material characterization and blade impact simulation," 2022.

[16] B. Hutchinson, "Critical assessment 16: Anisotropy in metals," *Materials Science and Technology*, vol. 31, no. 12, p. 1393–1401, Sep. 2015. [Online]. Available: http://dx.doi.org/10.1179/1743284715Y.0000000118

[17] B. Mooney, K. I. Kourousis, and R. Raghavendra, "Plastic anisotropy of additively manufactured maraging steel: Influence of the build orientation and heat treatments," *Additive Manufacturing*, vol. 25, p. 19–31, Jan. 2019. [Online]. Available: http://dx.doi.org/10.1016/j.addma.2018.10.032

[18] HBK, "The wheatstone bridge circuit explained," https://www.hbkworld.com/en/knowledge/resource-center/articles/strain-measurement-basics/strain-gauge-fundamentals/wheatstone-bridge-circuit [Accessed: (october 2023)].

[19] MTS, "Materials Test Systems," 2024, https://www.mts.com/en/products/materials [Accessed: (october 2024)].

[20] MakeItFrom, "Annealed grade 350 maraging steel," https://www.makeitfrom.com/material-properties/Annealed-Grade-350-Maraging-Steel [Accessed: (december 2023)].

[21] J. Foster, D. Frew, M. Forrestal, E. Nishida, and W. Chen, "Shock testing accelerometers with a hopkinson pressure bar," *International Journal of Impact Engineering*, vol. 46, pp. 56–61, 2012. [Online]. Available: https://www.sciencedirect.com/science/article/pii/S0734743X12000401

[22] Ansys, "Ls-dyna product space," https://lsdyna.ansys.com/ [Accessed: (2024)].

[23] Livermore Software Technology, "Ls-dyna, keyword user's manual, volume ii material models," 09 2021.

[24] B. O'Toole, M. Trabia, R. Hixson, S. K. Roy, M. Pena, S. Becker, E. Daykin, E. Machorro, R. Jennings, and M. Matthes, "Modeling plastic deformation of steel plates in hypervelocity impact experiments," *Procedia Engineering*, vol. 103, p. 458–465, 2015. [Online]. Available: http://dx.doi.org/10.1016/j.proeng.2015.04.060

[25] DYNAMORE, "Ls-opt," https://www.dynamore.se/en/products/opt/ls-op [Accessed: (2024)].

DEPARTMENT OF INDUSTRIAL AND MATERIALS SIENCE
CHALMERS UNIVERSITY OF TECHNOLOGY
Gothenburg, Sweden
www.chalmers.se

CHALMERS
UNIVERSITY OF TECHNOLOGY